Polymer Chemistry

PAPER

Check for updates

Mussel-inspired zwitterionic copolyethers for antifouling biomedical surfaces†

Minjung Kim, ‡[a] Minseong Kim,‡[a] Woojin Choi,[b] Milae Lee,[b] Jieun Kim,[c] Yeiji Kim,[c] Kyung Hyun Kim,[d] Ji Yeoun Lee,[c,d] Jinkee Hong[b] and Byeong-Su Kim *[a]

Owing to their superior hydrophilicity, zwitterionic molecules are known to form a strong hydration layer serving as an effective antifouling barrier. Despite their widespread use, the immobilization of zwitterionic molecules on various surfaces has posed a considerable challenge. Herein, we designed zwitterionic polyethers functionalized with mussel-inspired catechol moieties, which can be applied as versatile coatings with enhanced antifouling properties for biomedical surfaces. A series of block polyethers were synthesized *via* sequential anionic ring-opening polymerization of catechol-acetonide glycidyl ether and *N,N*-diisopropyl ethanolamine glycidyl ether, followed by post-polymerization modification to afford the desired zwitterionic brushes. The versatile surface adsorption and superior antifouling effects of the synthesized polyether brushes were evaluated using atomic force microscopy, quartz crystal microbalance with dissipation, and bioassay on the biomedical device surfaces. This study highlights the superior antifouling properties of zwitterionic polyether brushes, with potential applications in biomedical surfaces.

Introduction

Biofouling denotes the undesirable accumulation of proteins and microorganisms on various surfaces and devices.[1,2] This process reduces the performance and/or increases the operating costs of devices, including bioseparation and marine equipment. Furthermore, it poses significant challenges, particularly for the biomedical industry, which can potentially lead to life-threatening incidents such as contamination of medical devices and implants.[3,4] Therefore, improving the antifouling properties of biomedical devices has become a vital task to the avoid aforementioned issues and the resulting lethality.[5,6]

In this context, various approaches have been proposed to prevent biofouling, including antifouling paints[7] and sol–gel,[8] biocide-releasing,[9] or photocatalytic coatings.[10] Among these systems, various polymers have been used as nontoxic and antifouling surface-coating materials because of their high stability and tunability with unique functionalities. In particular, poly(ethylene glycol) (PEG)-based polymers have been most widely used in antifouling coatings, owing to their flexibility, biocompatibility, and high degree of hydration.[11–15] It is well known that surfaces coated with PEG prevent protein adsorption and cell adhesion because of the large excluded hydrodynamic volume caused by surface-bound water molecules upon the formation of a hydrogen-bonded hydration layer.[16] In addition, sulfur-containing copolymers have been widely used for antifouling and antibacterial surface coatings. The sulfide monomer can be ionized to carry positive charges, thus rendering surfaces with dual functions.[17]

Alternatively, zwitterions have been suggested as exceptional antifouling materials possessing a surface hydration layer with a similar function to that of PEG;[16,18] however, several studies have indicated that charged zwitterion-coated surfaces provide more robust antifouling properties due to their higher resistance to charged proteins and the stronger hydration layer formed in water *via* ionic interactions.[18–21] The surfaces of zwitterionic polymers do not perturb the native hydrogen bond network of water molecules in the vicinity of the surface. In contrast, the ionic groups and counterions of polyelectrolytes strongly perturb the structure of water molecules in their hydration shells. This led to the suggestion that the presence of the native hydrogen bond network of water near the surface is a critical feature to achieve antifouling and biocompatible properties.[22] Another noteworthy study investigated the surface hydration behavior of sulfobetaine methacrylate and oligo(ethylene glycol)methacrylate polymer brushes in

*a*Department of Chemistry, Yonsei University, Seoul 03722, Republic of Korea.
E-mail: bskim19@yonsei.ac.kr
*b*Department of Chemical and Biomolecular Engineering, College of Engineering, Yonsei University, Seoul 03722, Republic of Korea
*c*Department of Anatomy and Cell Biology, Seoul National University College of Medicine, Seoul 03080, Republic of Korea
*d*Department of Neurosurgery, Seoul National University Hospital, Seoul National University College of Medicine, Seoul 03080, Republic of Korea
†Electronic supplementary information (ESI) available. See DOI: https://doi.org/10.1039/d3py01286g
‡These authors contributed equally to this work.

contact with proteins.[23] The sum frequency generation vibrational spectroscopy revealed that the hydration layer on the zwitterionic sulfobetaine surface was not affected by the proteins, whereas that on the oligo(ethylene glycol) surface was significantly perturbed. While strong hydrogen bonds with water are formed by both the hydrophilic zwitterionic groups of sulfobetaine and the oxygen atoms of oligo(ethylene glycol), the strength of the hydrogen bonds in the former is enhanced by electrostatic attraction, thus enabling more effective surface hydration than in the latter. Moreover, the hydration free energies of zwitterionic carboxybetaine and sulfobetaine were calculated to be much lower than that of nonionic oligo(ethylene glycol) moieties, indicating that the zwitterionic materials exhibit stronger hydration.[24] It was also suggested that the highly charged groups avoid interactions with proteins, in contrast with the amphiphilic behavior of PEG materials that preferentially cover the hydrophobic domains of proteins in aqueous solution.[25]

Notwithstanding the superior antifouling properties of zwitterionic polymers, their immobilization onto target surfaces presents another challenge.[26,27] To date, these issues have primarily been addressed by surface-specific modifications. In alternative, a versatile surface coating strategy based on catechol moieties inspired by mussel-adhesive proteins could provide robust adhesion independent of the type of substrates.[28,29] This versatility has been widely exploited in various applications, such as adhesives,[30] surface coatings,[28] hydrogels,[31] surface primers,[32] nanoparticle modification agents, and sensors.[33]

In this context, we report herein the design of zwitterionic polyethers functionalized with mussel-inspired catechol moieties for versatile surface coatings with excellent antifouling properties (Scheme 1). Specifically, a series of block polyethers were synthesized via sequential anionic ring-opening polymerization (AROP) of catechol acetonide glycidyl ether (CAGE) and N,N-diisopropyl ethanolamine glycidyl ether (DEGE), followed by post-polymerization modification (PPM) to afford the desired zwitterionic brushes. To compare the antifouling effects of the zwitterionic brushes, we studied three different block polyethers with a constant catechol content. The versatile surface adsorption and superior antifouling effects of the synthesized polyether brushes were evaluated using atomic force microscopy (AFM), static contact angle measurements, quartz crystal microbalance with dissipation (QCM-D), and bioassay on the biomedical device surfaces such as poly(ethylene terephthalate glycol) (PETG) and Lyoplant, pure collagen dura mater substitute material. This study demonstrates the superior antifouling properties of zwitterionic polyether brushes, highlighting their promising application potential in biomedical surfaces.

Experimental section

Materials

p-Toluene sulfonic acid monohydrate (*p*-TsOH), benzene, tetrabutylammonium bromide (TBAB), tetrabutylammonium hydrogen sulfate (TBAHS), 2-(diisopropylamino)ethanol,
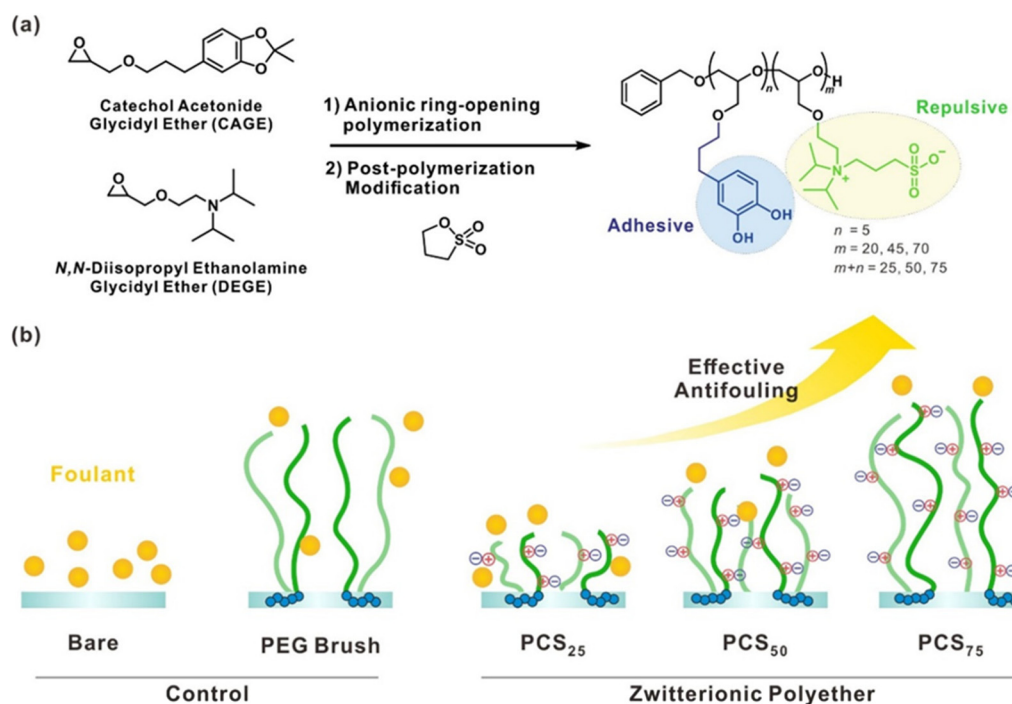
Scheme 1 Schematic representation of (a) synthesis and (b) antifouling behavior of zwitterionic copolyethers. Bare substrate and uncharged PEG brush were used as controls.

benzyl alcohol, *t*-Bu-P$_4$ phosphazene base solution (0.8 M in hexane), bovine serum albumin (BSA), phosphate-buffered saline (PBS, pH 7.4), formaldehyde, and toluene were obtained from Sigma-Aldrich. 3-(3,4-Dihydroxyphenyl)propionic acid (C-COOH), 2,2-dimethoxypropane, 1,3-propane sultone, and aluminum oxide were purchased from Alfa-Aesar. Lithium aluminum hydride (LiAlH$_4$) and epichlorohydrin (ECH) were obtained from Tokyo Chemical Industry. Potassium hydroxide flakes and 50% sodium hydroxide aqueous solution were obtained from Daejung, whereas 4′,6-diamidine-2′-phenylindole dihydrochloride (DAPI) and Alexa Fluor 488 were purchased from Thermo Fisher Scientific, USA. C2C12 (mouse embryonic myoblast) cells were purchased from American Type Culture Collection (ATCC). Deuterated NMR solvents including chloroform (CDCl$_3$) and methanol (MeOD) were purchased from Cambridge Isotope Laboratories. All chemicals were of analytical reagent grade and were used without purification, unless otherwise indicated.

Characterizations

^{1}H and ^{13}C NMR spectra were recorded on a Bruker 400 MHz spectrometer at 298 K. All spectra were recorded in ppm using CDCl$_3$ and MeOD. Gel permeation chromatography (GPC) measurements were performed on a JASCO CO-2060 Plus instrument equipped with KF-404HQ columns (Shodex, Tokyo, Japan), using chloroform (CHCl$_3$) as eluent and a UV detector. Polystyrene (PS) standards were used for calibration to determine the number-average (M_n) and weight-average (M_w) molecular weights, as well as the molecular weight dispersity (M_w/M_n, $Đ$). Aqueous GPC measurements were performed with a Cytiva Fast protein liquid chromatography (FPLC), with Superose™ 6, 10/300 GL as a solvent using PEG standards. FT-IR spectra were recorded on an Agilent Cary 630 spectrometer equipped with an attenuated total reflection (ATR) module. Differential scanning calorimetry (DSC) measurements were performed on a TA Instruments DSC 25 analyzer under nitrogen atmosphere, in the temperature range from −80 to 100 °C at a heating rate of 5 °C min^{-1}. The surface morphologies of the polymer-coated surfaces were investigated by AFM (NX10, Park Systems) in non-contact mode. Contact angles were determined using a Phoenix 300 goniometer (Surface Electro Optics Co. Ltd, Suwon, Korea). Real-time adsorptions of polymers and proteins were measured by a Q-sense E4 system (Biolin Scientific, Stockholm, Sweden).

Synthesis of catechol acetonide glycidyl ether (CAGE) monomer

The CAGE monomer was synthesized according to the method reported by Shin *et al.*,[11] with slight modifications. A mixture of 40% aqueous KOH (15.0 g, 0.27 mol, 10.0 equiv.), ECH (9.93 g, 107 mmol, 4.0 equiv.), and TBAHS (0.46 g, 1.34 mmol, 0.05 equiv.) was stirred vigorously at 0 °C. To this reaction mixture, 2,2-dimethyl-1,3-benzodioxole-5-propanol (CAOH, 5.59 g, 26.8 mmol, 1.0 equiv.) was slowly added and stirred for 6 h. Excess water was added to dilute the reaction mixture and extracted with diethyl ether. The organic phase was dried with

MgSO$_4$ and concentrated to obtain a pale-yellow, oily product. The crude product was purified using silica gel column chromatography with ethyl acetate/hexane (1 : 8 v/v) as the eluent to afford the catechol-functionalized CAGE monomer. The latter was distilled over CaH$_2$ before polymerization to give the pure product. Yield: 71.6%. ^{1}H NMR (400 MHz, CDCl$_3$): δ (ppm) 6.71–6.49 (m, 1H), 3.70 (dt, J = 13.1, 6.6 Hz, 1H), 3.48 (qt, J = 9.3, 6.4 Hz, 1H), 3.40–3.29 (m, 1H), 3.15 (ddt, J = 5.8, 4.1, 2.8 Hz, 1H), 2.79 (dd, J = 5.0, 4.2 Hz, 1H), 2.68–2.48 (m, 1H), 1.94–1.76 (m, 1H), 1.72–1.52 (m, 2H). ^{13}C NMR (101 MHz, CDCl$_3$): δ [ppm] 147.40, 145.48, 134.97, 120.51, 117.45, 108.69, 107.87, 71.50, 70.55, 50.84, 44.25, 31.98, 31.54, 25.82. Electrospray ionization mass spectrometry (ESI-MS) (m/z): C$_{15}$H$_{20}$O$_4$Na ([M + Na]$^+$), calcd 287.31, found 287.13.

Synthesis of *N,N*-diisopropyl ethanolamine glycidyl ether (DEGE) monomer

A mixture of 40% aqueous NaOH (72.7 mL, 1.00 mol, 10.0 equiv.), ECH (37.0 g, 400 mmol, 4.0 equiv.), and TBAB (1.61 g, 5.00 mmol, 0.05 equiv.) was stirred vigorously at 0 °C. To this reaction mixture, 2-(diisopropylamino)ethanol (14.5 g, 100 mmol, 1.0 equiv.) was slowly added and stirred for 4 h. Excess water was added to dilute the reaction mixture and extracted with diethyl ether. The organic phase was dried with MgSO$_4$ and concentrated to obtain a pale-yellow product. The crude product was distilled over CaH$_2$ before polymerization to give the pure product. Yield: 60.8%. ^{1}H NMR (400 MHz, CDCl$_3$): δ (ppm) 3.72 (dd, J = 11.4, 3.1 Hz, 1H), 3.44 (ddd, J = 14.9, 7.6, 4.1 Hz, 3H), 3.14 (td, J = 6.3, 3.2 Hz, 1H), 2.99 (dt, J = 13.0, 6.5 Hz, 2H), 2.80 (t, J = 4.6 Hz, 1H), 2.62 (dd, J = 9.0, 5.7 Hz, 3H), 1.01 (t, J = 7.1 Hz, 12H). ^{13}C NMR (101 MHz, CDCl$_3$): δ (ppm) 72.95, 71.67, 50.71, 49.34, 44.64, 44.20, 20.66. ESI-MS (m/z): C$_{11}$H$_{23}$NO$_2$H ([M + H]$^+$), calcd 202.32, found 202.18.

Synthesis of P(CAGE-*b*-DEGE) block copolymers

A series of protected catechol-functionalized polymers were synthesized by AROP with varying degrees of polymerization of DEGE. Taking poly(catechol acetonide glycidyl ether-*block-N,N*-diisopropyl ethanolamine glycidyl ether) [P(CAGE$_5$-*b*-DEGE$_{20}$), PCD$_{25}$], as an example, a mixture of *t*-BuP$_4$ (0.8 M in hexane, 0.48 mL, 0.38 mmol) and benzyl alcohol (39.0 μL, 0.38 mmol) in 1.25 mL of toluene was stirred for 30 min. Each of the glycidyl ether monomers was added in sequence at room temperature. First, CAGE (500 mg, 1.89 mmol) was slowly added to the solution to initiate the polymerization, while the reaction was monitored by ^{1}H NMR. When the residual epoxide signals of CAGE disappeared (within 3 h), DEGE (1.52 g, 7.57 mmol) was slowly added to the reaction mixture. The reaction was deemed complete when the residual epoxide signals of DEGE disappeared, as determined by ^{1}H NMR. Polymerization was terminated by adding benzoic acid (46.4 mg, 0.38 mmol), after which the mixture was passed through a basic alumina pad using THF to remove *t*-BuP$_4$. The solvent was evaporated to obtain poly(catechol acetonide glycidyl ether-*block-N,N*-diisopropyl ethanolamine glycidyl ether) [P(CAGE$_5$-*b*-DEGE$_{20}$), PCD$_{25}$]. ^{1}H NMR (400 MHz, CDCl$_3$): δ (ppm) 6.65–6.48 (m, 1H),

4.52 (s, 1H), 3.08–2.82 (m, 1H), 2.58 (s, 1H), 1.82 (d, $J = 17.6$ Hz, 1H), 1.63 (s, 1H), 1.05–0.90 (m, 7H). ^{13}C NMR (101 MHz, CDCl$_3$): δ (ppm) 147.33, 145.39, 128.33, 127.58, 120.48, 108.68, 107.85, 70.53 (d, $J = 513.8$ Hz), 49.42, 44.80, 32.08, 25.72 (d, $J = 23.3$ Hz), 21.93–18.64 (m).

Synthesis of P(CGE-b-SB) block copolymers

PCD$_{25}$ (300 mg, 0.06 mmol) was dissolved in 11 mL of MeOH, and 1,3-propane sultone (671 mg, 5.50 mmol) was added to the reaction mixture, followed by stirring vigorously at 60 °C for 16 h. During this process, the removal of the acetonide group was proceeded simultaneously to convert the PCAGE block to the deprotected PCGE block in poly(catechol glycidyl ether-block-sulfobetaine) [P(CGE$_5$-b-sulfobetaine$_{20}$), PCS$_{25}$]. Excess solvent was then removed using a rotary evaporator and the mixture was subsequently precipitated into cold diethyl ether. The PCS$_{25}$ polymer was dried using a vacuum to give a quantitative yield. ^1H NMR (400 MHz, MeOD): δ (ppm) 7.34 (s, 1H), 6.59 (d, $J = 41.7$ Hz, 1H), 4.54 (s, 1H), 4.04–3.22 (m, 24H), 3.00–2.72 (m, 2H), 2.54 (s, 1H), 2.15–1.92 (m, 2H), 1.81 (s, 1H), 1.43 (t, $J = 6.7$ Hz, 9H).

Static contact angle measurements

The static contact angles of water on the coated substrates were measured to analyze surface modifications. A SiO$_2$ substrate was cleaned prior to use and then incubated with the polymer solution (5.0 mg mL^{-1} in 70% ethanol) at room temperature for 24 h. After incubation, the substrate was washed five times with ethanol and dried with nitrogen. All samples were analyzed at least five times, and average values with the standard deviation as the error range is reported.

Polymer and protein adsorption tests using QCM-D

Real-time surface adsorption measurements were carried out using a gold-coated sensor (QSX 301, Biolin scientific). The sensor was transferred to a standard Q-sense flow module and equilibrated using 1× PBS before polymer injection. The flow rate was 600 μL min^{-1}, and the temperature was controlled at 25 °C in all experiments. The Voigt model was adopted to calculate the mass of adsorbed proteins with the Qtools software (Q-Sense, Sweden). The density of the adsorbed BSA layer, fluid density, and fluid viscosity were assumed to be 1200 kg m^{-3}, 1000 kg m^{-3}, and 0.001 kg ms^{-1}, respectively.

Cytotoxicity tests

C2C12 (mouse embryonic myoblast) cells were used for the cell attachment tests. Before various evaluations, the C2C12 cells were stabilized by incubation at 37 °C in a humidified incubator with 5% CO$_2$ in Dulbecco's modified Eagle's medium (DMEM) supplemented with 10% fetal bovine serum. After dip-coating each polymer over a PETG surface with an area of 1 × 1 cm^2, the loosely bound polymers were washed with 70% ethanol. The prepared specimens were thoroughly sterilized by 24 h exposure to UV radiation and transferred to a 24-well culture plate. A D-Plus CCK cell viability assay kit (Dongin LS, Korea) was used to monitor the cytotoxicity of C2C12 cells with

an initial seeding density of 5.0×10^4 cells per mL. To evaluate the cellular viability of attached C2C12, a 10% (v/v) CCK assay solution was treated and incubated for 2 h. The relative viability was measured by monitoring the optical density at 450 nm. The cytotoxicity of the adhered C2C12 cells was investigated 48 h after the initial seeding, following an identical protocol to the CCK assay.

In vitro cell adhesion test on PETG substrate

Polymer-coated PETG substrates were prepared as described above. C2C12 cells with a seeding density of 1.0×10^4 cells per mL were incubated for 48 h. Then, hemocytometer-based cell counting was conducted to quantify the absolute number of adhered cells. Furthermore, optical analysis was performed by the counterstaining method. Green (Alexa Fluor 488) and blue (4′,6-diamidino-2-phenylindole; DAPI) fluorescence dyes were used to visualize F-actin and nuclei, respectively. Before staining, the C2C12 cells were fixed on the surfaces using 10% (v/v) formaldehyde for 15 min at room temperature. Then, 0.2% Triton-X was applied for 15 min at room temperature to permeabilize C2C12. A mixture of 100 μM Alexa Fluor 488 and 50 μM DAPI solution was pre-incubated for 30 min at room temperature. The dilution medium consisted of 1× PBS solution with 1% BSA. Then, staining was performed for 20 min. Each procedure involved vigorous washing to obtain high-resolution images. Counterstained images were obtained with a confocal microscope (LSM 880, Carl Zeiss, USA).

In vitro cell adhesion test on Lyoplant substrate

A BJ-5TA fibroblast cell line was used in this study. Fibroblasts were cultured in a medium prepared by diluting high-glucose DMEM (Biowest, France) and M199 (Welgene, Republic of Korea) in a 4 : 1 ratio and adding 10% FBS, 1% penicillin/streptomycin (Thermo Fisher Scientific, USA), and 0.002% hygromycin B (Thermo Fisher Scientific, USA) at 37 °C in a humidified atmosphere with 5% CO$_2$. When the confluence reached about 70%, subculture was performed. The medium was changed every 3 to 4 days. Fibroblasts were used to evaluate cell adhesion onto bare (control) and coated Lyoplant (B. Braun, Germany; a bovine-derived, acellular and avascular material) using a 4-well slide chamber (SPL, Republic of Korea). Lyoplant was used as dura matter substitute material; it was cut according to the size of the well of the chamber and attached to the bottom of the well. Fibroblasts were dissociated and seeded on the Lyoplant surface at a density of 2×10^4 cells per cm^2. Then, they were incubated under standard cell culture conditions. After 6 h, the medium was aspirated, and the wells were washed twice with PBS. The samples were fixed using 4% paraformaldehyde solution for 5 min at room temperature and washed twice with PBS. Blue nucleic acid staining was performed with DAPI. Fibroblasts were stained with DAPI for 10 min at room temperature and washed twice with PBS; then, slides were mounted and imaged by fluorescence microscopy (Nikon, Japan). Five representative images were obtained for each sample, and cell counting was performed using the Image J software. All experiments were performed in
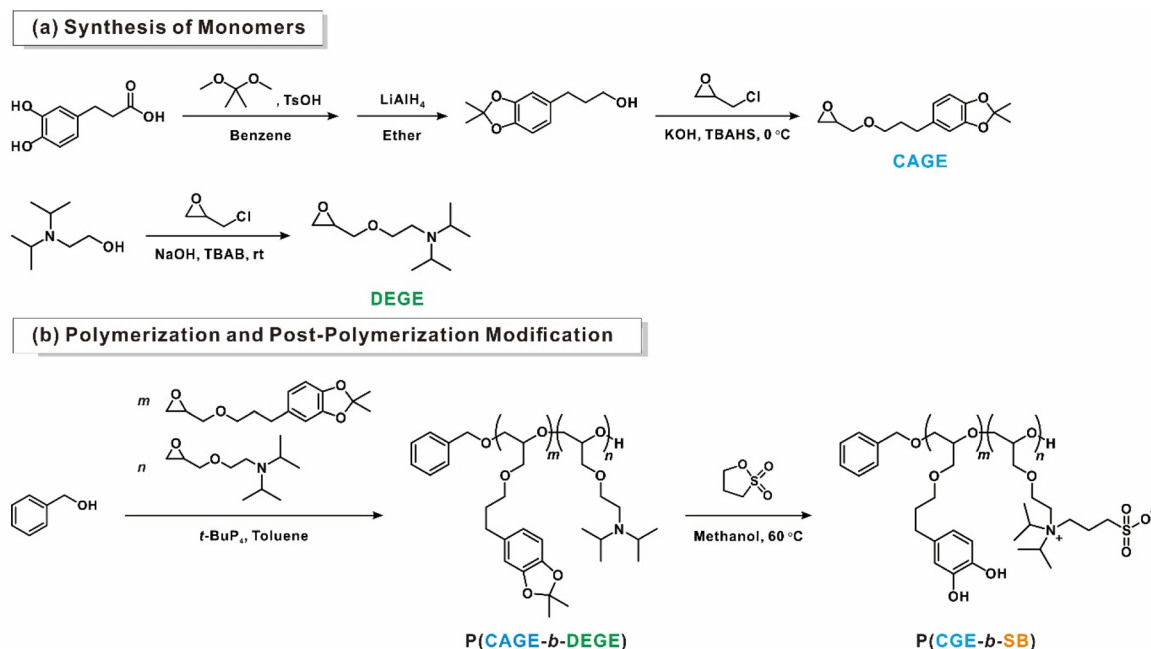
Scheme 2 (a) Preparation of the two functional epoxide monomers, CAGE and DEGE, and (b) block copolyethers prepared by anionic ring-opening polymerization followed by post-polymerization modification. See Experimental section for details.

triplicate. The experimental data were analyzed by one-way ANOVA followed by Scheffe and Duncan *post hoc* tests. Statistical significance was defined as a *p*-value of less than 0.05; standard error bars corresponded to 95% confidence intervals.

Results and discussion

Preparation and characterization of zwitterionic polyethers

Before preparing the zwitterionic polymers, the two types of functional epoxide monomers (CAGE and DEGE) were synthesized *via* simple steps to form functional polymers (Scheme 2). The CAGE monomer was selected as an adhesive moiety,[34,35] while DEGE was chosen as a precursor of the zwitterionic moiety.[36] Specifically, two glycidyl ether-based monomers, CAGE and DEGE, were obtained in moderate yields (71.6% and 60.8%, respectively) *via* a simple substitution reaction. Both monomers were purified by vacuum distillation over CaH_2 prior to polymerization. The successful syntheses of the two monomers were confirmed using ^{1}H, ^{13}C NMR, and heteronuclear single quantum coherence (HSQC) spectroscopy, as well as ESI-MS, respectively (Fig. 1a, b and Fig. S1–S8 in the ESI†).

Three different bifunctional block copolymers [poly(CAGE_{m}-b-DEGE_{n}), PCD_{m+n} in Table 1] were synthesized from the prepared monomers *via* AROP using benzyl alcohol as initiator and the metal-free organic base *t*-BuP₄ at 60 °C (Scheme 2b). The phosphazene base was previously reported to possess high basicity and low nucleophilicity, allowing the polymerization of the CAGE monomer to be achieved at a mild

temperature.[12] While phosphazene bases are highly effective in the controlled polymerization, it has been found that the residual phosphazene bases are detrimental to cell viability. Therefore, precise purification steps should be taken prior to the biomedical application of these polymers, as evidenced by the ^{31}P NMR analysis (Fig. S9†). Therefore, precise purification steps should be taken before the biomedical application of these polymers.

The sequential addition of the monomers yielded the desired block copolyethers in a controllable manner. The conversion of CAGE and DEGE was verified by monitoring the methine peak of the epoxide ring at 3.15 ppm using ^{1}H NMR spectroscopy. A series of precursor diblock (PCD) copolymers with three different molecular weights (5600–16 530 g mol⁻¹) were successfully prepared by controlling the monomer-to-initiator ratio (Table 1). It is of note that the degree of polymerization of the anchoring CAGE block was fixed to 5, which was found to be sufficient to immobilize the polymers onto the surface, while the degree of polymerization of the DEGE block was varied (m = 20, 45, and 70) for controlling the antifouling effect by adjusting the brush length.[12]

The obtained PCD copolymers bearing protected catechol and amine groups were characterized by ^{1}H NMR and GPC (Fig. 1c, Fig. S10,† and Table 1). The representative ^{1}H NMR spectrum of the PCD_{25} copolymer (entry 1 in Table 1) showed peaks corresponding to benzylic protons (4.57–4.55 ppm), aromatic protons of CAGE (6.91–6.51 ppm), polyether backbone (3.67–3.24 ppm), methine group of DEGE (3.05–2.85 ppm), methyl group of DEGE (1.02–0.95 ppm), and acetonide (1.66 ppm) (Fig. 1c). Moreover, the GPC trace of the PCD copolymers showed a monomodal distribution with narrow disper-
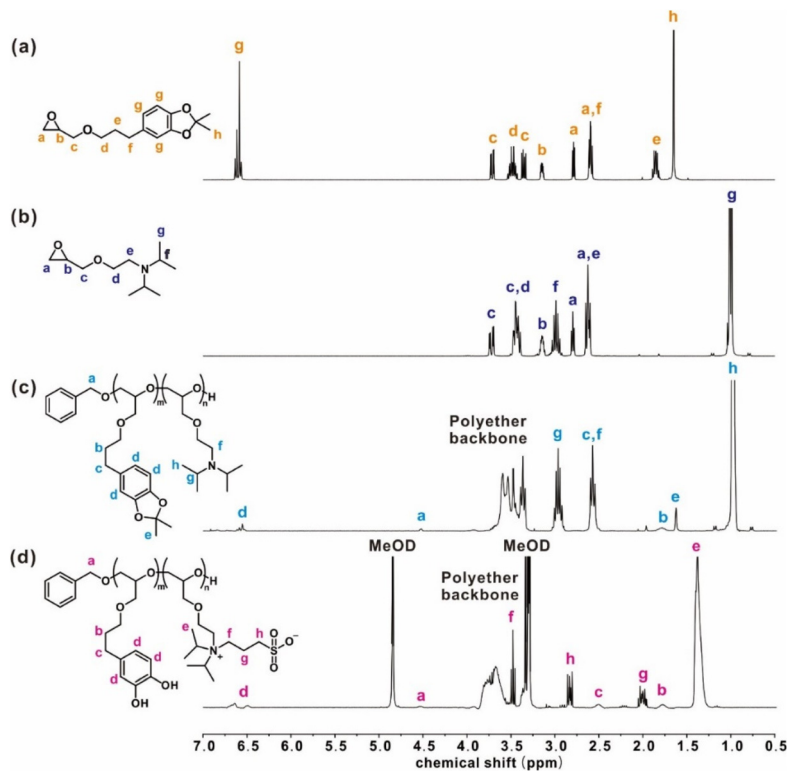
Fig. 1 Representative ^{1}H NMR spectra of (a) CAGE monomer, (b) DEGE monomer, (c) P(CAGE$_5$-b-DEGE$_{20}$) (PCD$_{25}$, entry 1 in Table 1), and (d) P(CGE$_5$-b-SB$_{20}$) (PCS25, entry 4 in Table 1).

Table 1 Characterization of the synthesized polyethers

		DP$_{n,NMR}$[a]				
Entry	Polymer composition	CAGE	DEGE	$M_{n,NMR}$ (g mol^{-1})	$M_{n,GPC}$ (g mol^{-1})	Đ
PEG brush[b]	P(TEG$_{45}$-b-CAG$_5$)[12]	5	45(TEG)	11 300	3800	1.11
PCD$_{25}$	P(CAGE$_5$-b-DEGE$_{20}$)	5	20	5600	2310[d]	1.13[d]
PCD$_{50}$	P(CAGE$_5$-b-DEGE$_{45}$)	5	45	10 490	2400[d]	1.15[d]
PCD$_{75}$	P(CAGE$_5$-b-DEGE$_{70}$)	5	70	16 530	1600[d]	1.31[d]
PCS$_{25}$	P(CGE$_5$-b-SB$_{20}$)[c]	5	20	7890	6920[e]	1.05[e]
PCS$_{50}$	P(CGE$_5$-b-SB$_{45}$)[c]	5	45	15 980	15 810[e]	1.05[e]
PCS$_{75}$	P(CGE$_5$-b-SB$_{70}$)[c]	5	70	25 070	26 760[e]	1.05[e]

[a] Degree of polymerization of CAGE and DEGE monomers. [b] PEG brush: P(TEG$_{45}$-b-CAG$_5$) with triethylene glycol glycidyl ether (TEG) monomer.[12] [c] CGE denotes the deprotected CAGE monomer. [d] Determined from GPC measurements (CHCl$_3$, PS standard). [e] Determined from GPC measurements (H$_2$O, PEG standard).

sity (Đ = 1.13–1.31), as obtained using the PS standard in CHCl$_3$. However, $M_{n,GPC}$ showed a significantly different tendency from $M_{n,NMR}$, possibly due to the presence of the tertiary amine moiety in the DEGE block that can strongly interact with the solid particles in the column. Thus, further analysis was carried out by GPC in water after the PPM.

Post-polymerization modifications

The pendant amine moieties of PCD polymers were transformed into the zwitterionic polyether poly(CGE-b-sulfobetaine) (PCS) *via* a simple ring-opening reaction of the DEGE

moiety with 1,3-propane sultone at 60 °C (Scheme 2b). Notably, the strong acid formed in this reaction resulted in the simultaneous deprotection of the acetonide protecting group in the CAGE block, leading to the successful formation of the desired antifouling zwitterionic PCS brushes at once. The formed zwitterionic PCS was characterized by ^{1}H NMR and GPC (Fig. 1d and Fig. S11†). A representative ^{1}H NMR spectrum of the zwitterionic polyethers showed peaks corresponding to three distinct methylene groups; one adjacent to the ammonium group (3.52–3.48 ppm), one in the middle of the chain (2.05–2.02 ppm), and one adjacent to the sulfonyl

groups (2.83–2.75 ppm), along with the disappearance of the acetonide peak (1.66 ppm) from the CAGE block (Fig. 1d). Moreover, the GPC trace of the zwitterionic polymers (obtained using the PEG standard in water) showed a monomodal distribution with narrow dispersity ($Đ$ = 1.05). Hence, the exact molecular weights were determined by GPC in deionized (DI) water after PPM, which clearly shifted to the higher-molecular-weight region with increasing molecular weight. The characterizations of the synthesized polymers are listed in Table 1. It is noteworthy that, despite the presence of low-molecular-weight homopolymers evidenced by the GPC traces, their contribution to the overall antifouling performance of the resulting polymers is very limited. While the initial PCDs were soluble in several organic solvents, the zwitterionic polyethers (*i.e.*, PCS) prepared after PPM displayed a markedly different solubility, indicating the completion of the ring-opening reaction of the sultone.

Furthermore, the successful polymerization and modification were confirmed by FT-IR spectroscopy (Fig. S12†). For example, the main bands in the ranges of 1060–1080 cm^{-1} and 2850–2930 cm^{-1} were attributed to the polyether backbone. After deprotection of the acetonide group, a broad signal characteristic of hydroxyl groups appeared at 3650–3100 cm^{-1}. Moreover, the successful PPM was revealed by the appearance of the characteristic sulfonyl peaks at 1035 and 750 cm^{-1}, attributed to the symmetric stretching vibrations of S═O and S–O bands. DSC measurements showed different glass transition temperatures (T_g) for the PCD$_{25}$ and PCS$_{25}$ polymers (Fig. S13†). The T_g value of the PCD$_{25}$ and PCS$_{25}$ polymers increased significantly from −47 to −4 °C, indicating the presence of stronger intermolecular interactions in the zwitterionic polyethers.

Characterization of surface coatings

After the successful synthesis of zwitterionic polyethers, the PCS solutions (5.0 mg mL^{-1} in 70% EtOH) were deposited on a silicon wafer as a model substrate, to induce the adsorption of polymers *via* a solution-dipping method. The surface coating of the PCS polymers was studied by measuring the static contact angle of water droplets after coating. While the bare silicon wafer showed a static contact angle of 65°, all three samples displayed more hydrophilic surfaces with reduced contact angles of 49.8 ± 1.8° (PCS$_{25}$), 46.6 ± 1.0° (PCS$_{50}$), and 41.4 ± 2.0° (PCS$_{75}$), suggesting a successful surface hydration upon coating with PCS polymers (Fig. 2a).

Additionally, the surface morphology of the polymer-coated surfaces was verified using AFM. The three substrates showed a relatively uniform and smooth surface morphology without significant nanostructures on the surface. The relatively low root-mean-square surface roughness (R_{rms}) values of 0.85–1.26 nm indicated a uniform coating of the PCS copolymer on the surface (Fig. 2b). The control set of acetonide-protected PCD polymer was readily rinsed away, demonstrating the critical role of the free catechol moiety in anchoring the polymers to the surface. Independent of the surface morphology of the polymer coated surfaces, ellipsometry measurements supported the formation of zwitterionic PCS polymer coatings with thicknesses of 4.17 ± 0.15 nm (PCS$_{25}$), 4.76 ± 0.27 nm (PCS$_{50}$), and 6.31 ± 0.53 nm (PCS$_{75}$). Moreover, it is worth noting that the surface morphology of the polymers was affected by the coating conditions and the type of rinsing solvent.

QCM-D analysis was employed to quantitatively assess the real-time antifouling performance by monitoring the adsorption of polymers and proteins onto the polymer-coated substrates (Fig. 3). Prior to coating the polymers, the bare gold substrate was equilibrated in flowing PBS buffer at pH 7.4 to attain steady frequency and dissipation baselines. Polymer coating was then carried out using the zwitterionic polymer solution (5.0 mg mL^{-1} in 70% EtOH) for 30 min, which generated a negative frequency shift, suggesting an increase in the
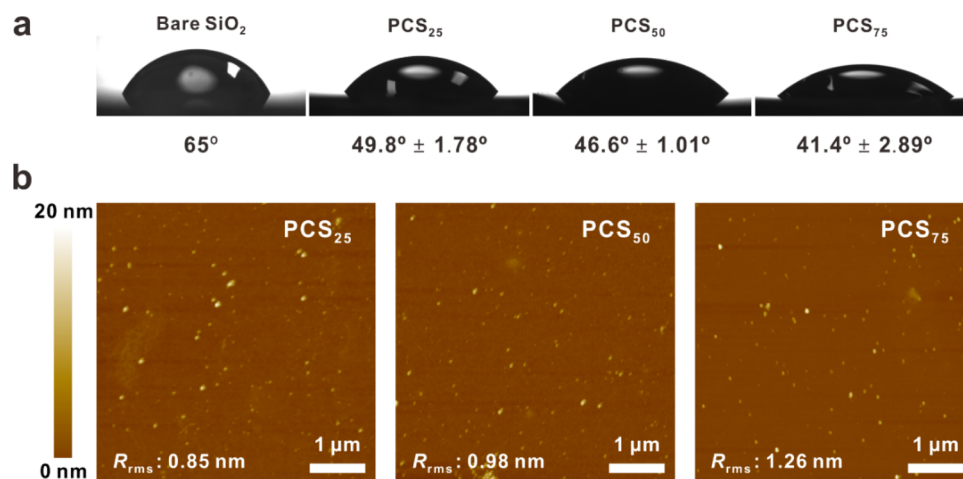
Fig. 2 (a) Static contact angles of water droplets on three different brushes (PCS$_{25}$, PCS$_{50}$, PCS$_{75}$) and bare surfaces. The average contact angle value for five repetitions is reported along with the standard deviation. (b) Representative topological AFM images of polymer coatings on silicon wafers (polymer concentration: 5.0 mg mL^{-1} in 70% EtOH). The root-mean-square roughness (R_{rms}) value was determined as the average of three independent measurements.
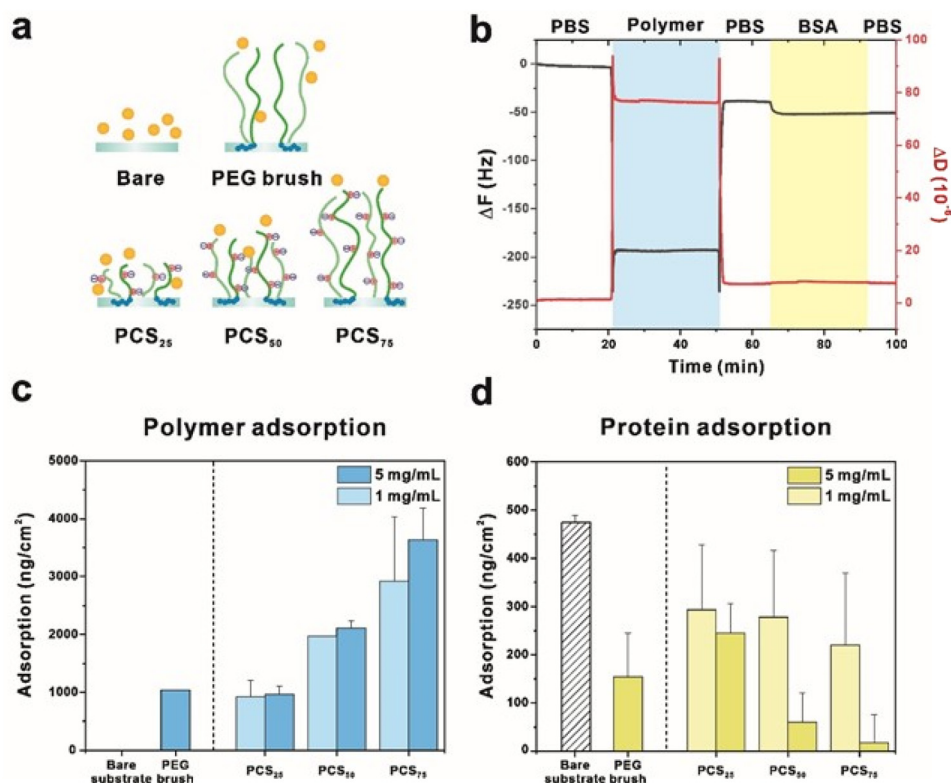
Fig. 3 (a) Schematic diagram of antifouling effect of PCS brushes in reference to bare substrate and uncharged PEG brush controls. (b) Representative changes in frequency (ΔF, black) and dissipation (ΔD, red) associated with the adsorption of zwitterionic PCS$_{75}$ polyether brush coated on a gold substrate, obtained from QCM-D measurements. (c) Adsorption of various polymer samples on bare gold substrates with different concentrations. (d) Adsorption of BSA on various polymer-coated gold substrates. For each experiment, three overtones with more than three measurements were used to calculate the average values and standard deviations. PEG brush: PEG brush: P(TEG$_{45}$-b-CAG$_5$).[12]

mass of the substrate after polymer coating. The steep slope of the ΔD vs. $\Delta F/n$ plot (i.e., 3.9×10^{-7} and 4.7×10^{-7} Hz^{-1} for the PCS$_{75}$ brush) demonstrated the viscoelastic behavior of the absorbed zwitterionic polymers on the substrate, similar to previous reports (Fig. S14–S16†). Thus, in this study we used the Voigt model in place of the conventional Sauerbrey equation to calculate the mass of the polymer deposited on the substrate (Fig. 3c). After coating the polymers, the loosely bound polymers were removed by additional PBS rinsing for 15 min, followed by the injection of BSA solution into the polymer-coated substrates. As a reference, we prepared the plain PEG brush of mPEG$_{114}$-b-PCGE$_4$ in which uncharged PEG brush is anchored onto the surface with identical catechol-based PCGE moiety according to our previous study.[11]

As shown in Fig. 3c, a similar amount of adsorbed PCS brushes was observed for the two different concentrations tested, while a higher polymer concentration of 5.0 mg mL^{-1} yielded a higher coverage of the substrate with PCS brushes. Moreover, the amount of adsorbed zwitterionic PCS brushes increased with increasing chain length of the brush polymers, from 962.20 ng cm^{-2} (PCS$_{25}$) to 2113.11 ng cm^{-2} (PCS$_{50}$) and 3638.33 ng cm^{-2} (PCS$_{75}$) (Table 2). For comparison, the amount of the PEG brush was determined to be 589.96 ± 190.06 ng cm^{-2}.

From the absorbed polymer mass on a given area of the substrate, the grafting density (σ) of each polymer was extracted (Table 2). By comparing a series of zwitterionic polyethers anchored on the surface, it was found that the grafting density increased with the zwitterionic chain length; for example, σ values of 0.72, 0.79, and 0.88 chains per nm^2 were obtained for PCS$_{25}$, PCS$_{50}$, and PCS$_{75}$, respectively. As the grafting density of polymer brushes varies depending on the coating conditions, the brushes exhibit weak overlap and even no interactions (i.e., "mushroom" regime) at low concentrations.[37] However, polymer brushes with a higher grafting density at high concentrations display strong overlap and form outstretched and thick coating layers. These results often provide guidelines for controlling the conformational behavior of polymeric brushes on a surface.

In contrast to a previous study in which longer polymeric brushes showed a lower surface grafting density due to steric hindrance,[38] we found that the PCS$_{75}$ brush displayed the highest grafting density on the surface. This result likely originated from the strong inter- and intramolecular interactions between neighboring zwitterionic groups, which resulted in an increased surface adsorption of longer zwitterionic chains. Accordingly, one can anticipate that the PCS$_{75}$ brushes with a high polymer grafting density would form a thicker hydration

Table 2 Antifouling properties of zwitterionic polyethers

| Entry | Polymer composition | QCM-D[a] | | σ (chains per nm^2) |
		Polymer adsorption (ng cm^{-2})	BSA adsorption (ng cm^{-2})	
PCS$_{25}$	P(CGE$_5$-b-SB$_{20}$)	962.20 ± 145.68	245.23 ± 61.33	0.72
PCS$_{50}$	P(CGE$_5$-b-SB$_{45}$)	2113.11 ± 123.96	59.93 ± 60.54	0.79
PCS$_{75}$	P(CGE$_5$-b-SB$_{70}$)	3638.33 ± 548.34	17.90 ± 57.84	0.88

[a] The adsorbed mass and grafting density were measured by substituting the frequency into the Voigt model. Each polymer and protein were coated at a concentration of 5.0 mg mL^{-1} for 30 min and washed with PBS.

layer, which in turn lead to a more effective antifouling behavior.

Finally, we measured the mass of adsorbed BSA after injection of the corresponding solution. The mass of adsorbed BSA on the bare gold substrate (536.15 ng cm^{-2}) was significantly higher than that on PCS$_{25}$ (245.23 ng cm^{-2}), PCS$_{50}$ (59.93 ng cm^{-2}), and PCS$_{75}$ (17.90 ng cm^{-2}) (Table 2).

The comparison of PCS brushes with three different zwitterionic chain lengths showed that PCS$_{75}$ exhibited the lowest protein adsorption. It is also of note that the mass of BAS adsorbed on uncharged PEG brush (34.61 ± 39.37 ng cm^{-2}) was relatively higher than that of PCS$_{75}$, indicating the superior efficiency of zwitterionic coating. Combined with the trend of the grafting density, this suggests that polymers with a longer zwitterionic chain strongly favored the formation of the hydration layer necessary for the antifouling property.

Cell viability assay and antifouling tests

Finally, we evaluated the *in vitro* cytotoxicity of the zwitterionic polyethers and assessed their antifouling performance on model biomedical surfaces such as PETG and Lyoplant (Fig. 4). PETG was selected because it is widely employed in dental materials owing to its high biocompatibility, mechanical strength, and resistance against chemicals. In addition, Lyoplant was chosen as one of the most common materials used as dura mater substitute in neurosurgical operations, which often require materials with antifouling properties.

Cell attachment tests demonstrated the antifouling effect of the three different zwitterionic polyethers. The three polymers were dip-coated on both PETG and Lyoplant substrates for *in vitro* assay. In contrast with the uncoated PETG surfaces, a significant reduction in the number of adhered cells was
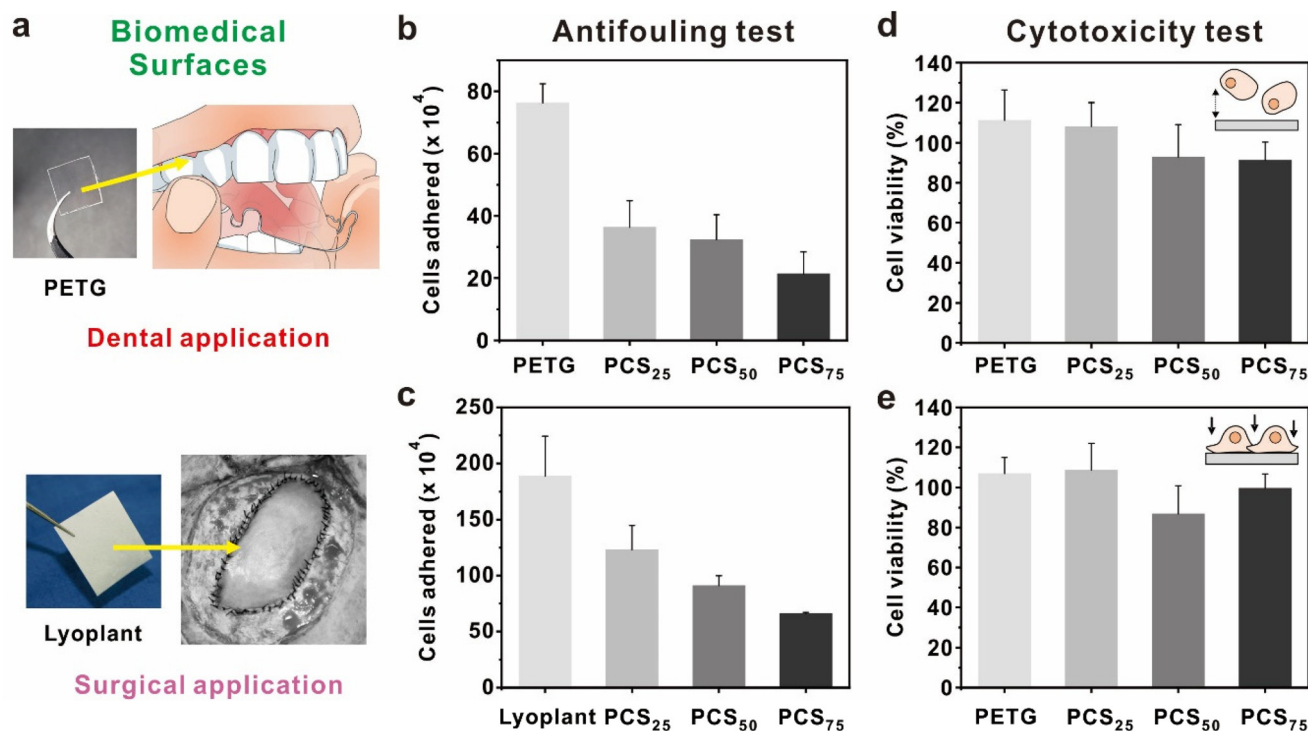
Fig. 4 *In vitro* evaluation of antifouling properties and viability of zwitterionic polyether brushes. (a) Images of model biomedical surfaces; (b and c) number of cells deposited on polymer-coated PETG (b) and Lyoplant (c) surfaces. (d and e) Cellular viability of (d) floating and (e) C2C12 cells adhered on polymer-coated PETG surface. Initial seeding density: 1.0×10^4 cell per mL.
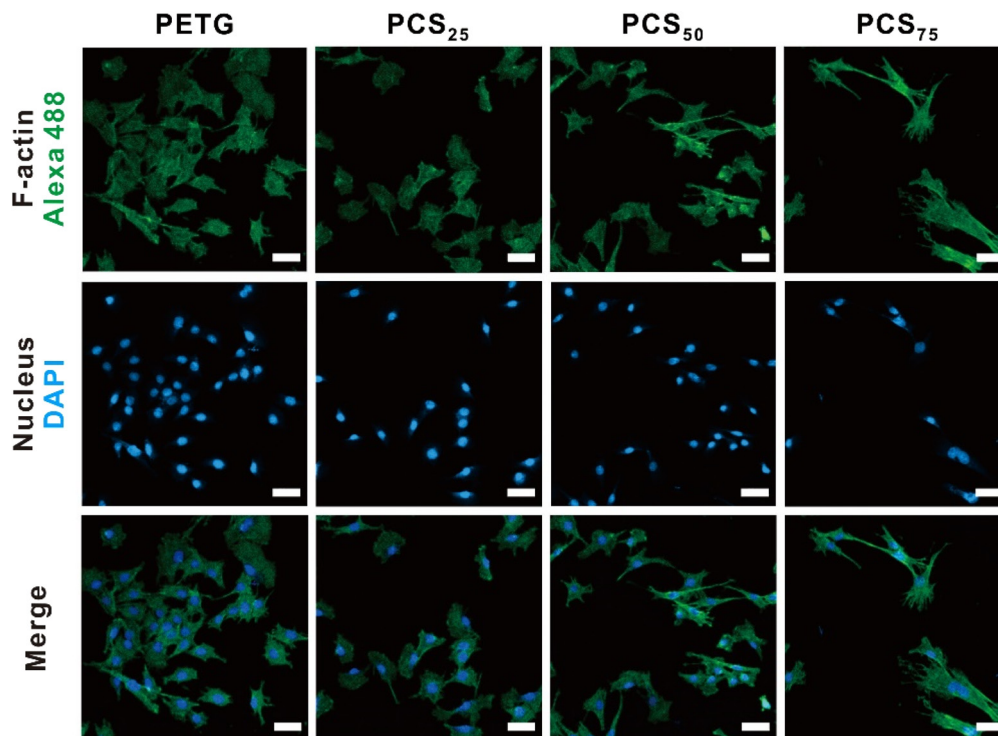
Fig. 5 Fluorescence microscopy images of Alexa Flour 488- and DAPI-stained cells deposited on PETG and polymer-coated PETG surfaces. Initial seeding density: 1.0×10^4 cell per cm^2. Scale bars: 50 μm.

observed for all three zwitterionic polymer-coated surfaces, clearly demonstrating the antifouling effect of the zwitterionic polyethers (Fig. 4b). PCS$_{75}$ displayed the strongest antifouling effect among the studied samples, in good agreement with the QCM-D results. Similarly, the antifouling effect of zwitterionic polyether-coated Lyoplant was evaluated using fibroblast cells. Although a relatively small difference was observed between the bare and PCS$_{25}$-coated substrates, PCS$_{50}$- and PCS$_{75}$-coated Lyoplant showed a significantly reduced number of adhered fibroblast cells compared to the bare substrate (Fig. 4c).

Furthermore, the polymer-coated substrates were placed in a 24-well plate, and C2C12 (mouse embryonic myoblast) cells were immediately seeded for 48 h to monitor the cytotoxicity and antifouling properties of each sample. The *in vitro* cell viability in the presence of the respective zwitterionic polyethers was studied *via* the CCK assay. Significant numbers of floating and adhered C2C12 cells were observed in both cases compared to the control, indicating the high biocompatibility of the zwitterionic polyether brush coatings (Fig. 4d and e).

Finally, the antifouling performances were evaluated by analyzing fluorescence microscopy images of the polymer-coated PETG substrates (Fig. 5). While the C2C12 fibroblasts showed normal adhesion and proliferation on the uncoated surface, most cells deposited on the zwitterionic polymer-coated surfaces were found to be reduced and were not colonized, as revealed by optical and fluorescence microscopy images. In particular, the total number of adhered fibroblasts was significantly reduced in the case of the PCS$_{75}$ sample,

revealing that the superior properties of the hydration layer resulted in the improved antifouling behavior.

Conclusions

In summary, a series of zwitterionic polyether brushes were designed and prepared by using two functional epoxide monomers, CAGE and DEGE, followed by post-polymerization modification to explore the effect of the chain length on the antifouling performance. The mussel-inspired catechol moiety allowed the versatile adsorption of the brushes on the surfaces, while the zwitterionic segment along with the highly hydrophilic polyether backbone imparted superior antifouling properties. Zwitterionic polyether brushes with a high polymer grafting density formed a thicker hydration layer, resulting in more effective antifouling behavior, as evidenced by QCM-D measurements. The versatile surface adsorption and superior antifouling effects of the synthesized zwitterionic polyether brushes were demonstrated on representative dental and medical surfaces, highlighting the promising application potential of the present systems.

Conflicts of interest

There are no conflicts to declare.

Acknowledgements

References

1 G. D. Bixler and B. Bhushan, Biofouling: Lessons from Nature, *Philos. Trans. R. Soc., A*, 2012, **370**, 2381–2417.

2 I. Davidson, C. Scianni, C. Hewitt, R. Everett, E. Holm, M. Tamburri and G. Ruiz, Mini-Review: Assessing the Drivers of Ship Biofouling Management–Aligning Industry and Biosecurity Goals, *Biofouling*, 2016, **32**, 411–428.

3 Q. Wei, T. Becherer, S. Angioletti-Uberti, J. Dzubiella, C. Wischke, A. T. Neffe, A. Lendlein, M. Ballauff and R. Haag, Protein Interactions with Polymer Coatings and Biomaterials, *Angew. Chem., Int. Ed.*, 2014, **53**, 8004–8031.

4 S. Jiang and Z. Cao, Ultralow–Fouling, Functionalizable, and Hydrolyzable Zwitterionic Materials and Their Derivatives for Biological Applications, *Adv. Mater.*, 2010, **22**, 920–932.

5 Q. Xin, Z. Ma, S. Sun, H. Zhang, Y. Zhang, L. Zuo, Y. Yang, J. Xie, C. Ding and J. Li, Supramolecular Self-Healing Antifouling Coating for Dental Materials, *ACS Appl. Mater. Interfaces*, 2023, **15**, 41403–41416.

6 J. Zhang, M. Wu, P. Peng, J. Liu, J. Lu, S. Qian and J. Feng, "Self-Defensive" Antifouling Zwitterionic Hydrogel Coatings on Polymeric Substrates, *ACS Appl. Mater. Interfaces*, 2022, **14**, 56097–56109.

7 E. Almeida, T. C. Diamantino and O. de Sousa, Marine Paints: The Particular Case of Antifouling Paints, *Prog. Org. Coat.*, 2007, **59**, 2–20.

8 M. R. Detty, R. Ciriminna, F. V. Bright and M. Pagliaro, Environmentally Benign Sol-Gel Antifouling and Foul-Releasing Coatings, *Acc. Chem. Res.*, 2014, **47**, 678–687.

9 A. Ali, M. I. Jamil, J. Jiang, M. Shoaib, B. U. Amin, S. Luo, X. Zhan, F. Chen and Q. Zhang, An Overview of Controlled-Biocide-Release Coating Based on Polymer Resin for Marine Antifouling Applications, *J. Polym. Res.*, 2020, **27**, 1–17.

10 R. Ciriminna, F. V. Bright and M. Pagliaro, Ecofriendly Antifouling Marine Coatings, *ACS Sustainable Chem. Eng.*, 2015, **3**, 559–565.

11 E. Shin, C. Lim, U. J. Kang, M. Kim, J. Park, D. Kim, W. Choi, J. Hong, C. Baig and D. W. Lee, Mussel-Inspired Copolyether Loop with Superior Antifouling Behavior, *Macromolecules*, 2020, **53**, 3551–3562.

12 S. Park, M. Kim, J. Park, W. Choi, J. Hong, D. W. Lee and B. S. Kim, Mussel-Inspired Multiloop Polyethers for Antifouling Surfaces, *Biomacromolecules*, 2021, **22**, 5173–5184.

13 C. Yang, X. Ding, R. J. Ono, H. Lee, L. Y. Hsu, Y. W. Tong, J. Hedrick and Y. Y. Yang, Brush-Like Polycarbonates Containing Dopamine, Cations, and Peg Providing a Broad-Spectrum, Antibacterial, and Antifouling Surface Via One-Step Coating, *Adv. Mater.*, 2014, **26**, 7346–7351.

14 S. C. Goh, Y. Luan, X. Wang, H. Du, C. Chau, H. E. Schellhorn, J. L. Brash, H. Chen and Q. Fang, Polydopamine-Polyethylene Glycol-Albumin Antifouling Coatings on Multiple Substrates, *J. Mater. Chem. B*, 2018, **6**, 940–949.

15 C. S. Gudipati, J. A. Finlay, J. A. Callow, M. E. Callow and K. L. Wooley, The Antifouling and Fouling-Release Perfomance of Hyperbranched Fluoropolymer (Hbfp)– Poly (Ethylene Glycol)(Peg) Composite Coatings Evaluated by Adsorption of Biomacromolecules and the Green Fouling Alga Ulva, *Langmuir*, 2005, **21**, 3044–3053.

16 B. K. D. Ngo and M. A. Grunlan, Protein Resistant Polymeric Biomaterials, *ACS Macro Lett.*, 2017, **6**, 992–1000.

17 X. Xu, Q. Wang, Y. Chang, Y. Zhang, H. Peng, A. K. Whittaker and C. Fu, Antifouling and Antibacterial Surfaces Grafted with Sulfur-Containing Copolymers, *ACS Appl. Mater. Interfaces*, 2022, **14**, 41400–41411.

18 Z. Cao and S. Jiang, Super-Hydrophilic Zwitterionic Poly (Carboxybetaine) and Amphiphilic Non-Ionic Poly (Ethylene Glycol) for Stealth Nanoparticles, *Nano Today*, 2012, **7**, 404–413.

19 Z. G. Estephan, P. S. Schlenoff and J. B. Schlenoff, Zwitteration as an Alternative to Pegylation, *Langmuir*, 2011, **27**, 6794–6800.

20 A. J. Keefe and S. Jiang, Poly (Zwitterionic) Protein Conjugates Offer Increased Stability without Sacrificing Binding Affinity or Bioactivity, *Nat. Chem.*, 2012, **4**, 59–63.

21 N. Erathodiyil, H.-M. Chan, H. Wu and J. Y. Ying, Zwitterionic Polymers and Hydrogels for Antibiofouling Applications in Implantable Devices, *Mater. Today*, 2020, **38**, 84–98.

22 S. Krishnan, C. J. Weinman and C. K. Ober, Advances in Polymers for Anti-Biofouling Surfaces, *J. Mater. Chem.*, 2008, **18**, 3405–3413.

23 C. Leng, H. C. Hung, S. Sun, D. Wang, Y. Li, S. Jiang and Z. Chen, Probing the Surface Hydration of Nonfouling Zwitterionic and Peg Materials in Contact with Proteins, *ACS Appl. Mater. Interfaces*, 2015, **7**, 16881–16888.

24 Q. Shao, Y. He, A. D. White and S. Jiang, Difference in Hydration between Carboxybetaine and Sulfobetaine, *J. Mater. Chem. B*, 2010, **114**, 16625–16631.

25 Q. Shao and S. Jiang, Molecular Understanding and Design of Zwitterionic Materials, *Adv. Mater.*, 2015, **27**, 15–26.

26 M. He, K. Gao, L. Zhou, Z. Jiao, M. Wu, J. Cao, X. You, Z. Cai, Y. Su and Z. Jiang, Zwitterionic Materials for Antifouling Membrane Surface Construction, *Acta Biomater.*, 2016, **40**, 142–152.

27 K. G. Neoh, M. Li, E. T. Kang, E. Chiong and P. A. Tambyah, Surface Modification Strategies for Combating Catheter-Related Complications: Recent Advances and Challenges, *J. Mater. Chem. B*, 2017, **5**, 2045–2067.

28 Q. Wei, K. Achazi, H. Liebe, A. Schulz, P. L. M. Noeske, I. Grunwald and R. Haag, Mussel–Inspired Dendritic Polymers as Universal Multifunctional Coatings, *Angew. Chem., Int. Ed.*, 2014, **53**, 11650–11655.

29 B. P. Lee, P. B. Messersmith, J. N. Israelachvili and J. H. Waite, Mussel-Inspired Adhesives and Coatings, *Annu. Rev. Mater. Res.*, 2011, **41**, 99–132.

30 J. Sedo, J. Saiz-Poseu, F. Busque and D. Ruiz-Molina, Catechol-Based Biomimetic Functional Materials, *Adv. Mater.*, 2013, **25**, 653–701.

31 J. H. Ryu, Y. Lee, W. H. Kong, T. G. Kim, T. G. Park and H. Lee, Catechol-Functionalized Chitosan/Pluronic Hydrogels for Tissue Adhesives and Hemostatic Materials, *Biomacromolecules*, 2011, **12**, 2653–2659.

32 E. Shin, S. W. Ju, L. An, E. Ahn, J. S. Ahn, B. S. Kim and B. K. Ahn, Bioinspired Catecholic Primers for Rigid and Ductile Dental Resin Composites, *ACS Appl. Mater. Interfaces*, 2018, **10**, 1520–1527.

33 A. Chaicham, S. Sahasithiwat, T. Tuntulani and B. Tomapatanaget, Highly Effective Discrimination of Catecholamine Derivatives Via Fret-on/Off Processes Induced by the Intermolecular Assembly with Two Fluorescence Sensors, *Chem. Commun.*, 2013, **49**, 9287–9289.

34 A. Thomas, H. Bauer, A.-M. Schilmann, K. Fischer, W. Tremel and H. Frey, The "Needle in the Haystack" Makes the Difference: Linear and Hyperbranched Polyglycerols with a Single Catechol Moiety for Metal Oxide Nanoparticle Coating, *Macromolecules*, 2014, **47**, 4557–4566.

35 K. Niederer, C. Schüll, D. Leibig, T. Johann and H. Frey, Catechol Acetonide Glycidyl Ether (Cage): A Functional Epoxide Monomer for Linear and Hyperbranched Multi-Catechol Functional Polyether Architectures, *Macromolecules*, 2016, **49**, 1655–1665.

36 A. Lee, P. Lundberg, D. Klinger, B. F. Lee, C. J. Hawker and N. A. Lynd, Physiologically Relevant, Ph-Responsive Peg-Based Block and Statistical Copolymers with N, N-Diisopropylamine Units, *Polym. Chem.*, 2013, **4**, 5735–5742.

37 P. Jungmann, T. Kreer, J.-U. Sommer and J. Paturej, Conformational Properties of End-Grafted Bottlebrush Polymers, *Macromolecules*, 2020, **54**, 161–169.

38 G. Morgese, L. Trachsel, M. Romio, M. Divandari, S. N. Ramakrishna and E. M. Benetti, Topological Polymer Chemistry Enters Surface Science: Linear Versus Cyclic Polymer Brushes, *Angew. Chem., Int. Ed.*, 2016, **55**, 15583–15588.